Optical Materials 42 (2015) 167–173

Contents lists available at ScienceDirect

Optical Materials

journal homepage: www.elsevier.com/locate/optmat

# Efficient upconversion-pumped continuous wave $Er^{3+}$:$LiLuF_4$ lasers

Francesca Moglia [a,*], Sebastian Müller [a], Fabian Reichert [a,b], Philip W. Metz [a], Thomas Calmano [a,c], Christian Kränkel [a,c], Ernst Heumann [a], Günter Huber [a,c]

[a] Institut für Laser-Physik, Universität Hamburg, Luruper Chaussee 149, 22761 Hamburg, Germany
[b] Center for Free-Electron Laser Science, DESY, Notkestraße 85, 22607 Hamburg, Germany
[c] The Hamburg Centre for Ultrafast Imaging, Luruper Chaussee 149, 22761 Hamburg, Germany

ARTICLE INFO

*Article history:*
Received 16 October 2014
Received in revised form 28 November 2014
Accepted 5 January 2015
Available online 13 February 2015

*Keywords:*
Laser materials
Upconversion lasers
Waveguide lasers

ABSTRACT

We report on detailed spectroscopic investigations and efficient visible upconversion laser operation of $Er^{3+}$:$LiLuF_4$. This material allows for efficient resonant excited-state-absorption (ESA) pumping at 974 nm. Under spectroscopic conditions without external feedback, ESA at the laser wavelength of 552 nm prevails stimulated emission. Under lasing conditions in a resonant cavity, the high intracavity photon density bleaches the ESA at 552 nm, allowing for efficient cw laser operation.

We obtained the highest output power of any room-temperature crystalline upconversion laser. The laser achieves a cw output power of 774 mW at a slope efficiency of 19% with respect to the incident pump power delivered by an optically-pumped semiconductor laser. The absorption efficiency of the pump radiation is estimated to be below 50%.

To exploit the high confinement in waveguides for this laser, we employed femtosecond-laser pulses to inscribe a cladding of parallel tracks of modified material into $Er^{3+}$:$LiLuF_4$ crystals. The core material allows for low-loss waveguiding at pump and laser wavelengths. Under Ti:sapphire pumping at 974 nm, the first crystalline upconversion waveguide laser has been realized. We obtained waveguide-laser operation with up to 10 mW of output power at 553 nm.



## 1. Introduction

Upconversion lasers are unconventional short-wavelength sources as, for instance, visible radiation can be achieved with the use of near infrared pump sources. Different rare-earth ions allow for upconversion lasers, e.g. trivalent neodymium, thulium, and praseodymium [1–3]. Many pumping schemes for upconversion lasers use more than one pump wavelength, which limits the compactness of these systems [1]. The goal of this work was the realization of green upconversion lasers pumped with one single wavelength around 970 nm, employing either Ti:sapphire or semiconductor lasers. A similar scheme was first realized in various $Er^{3+}$-doped materials by Johnson et al., although the pump source was a flash lamp and co-doping with $Yb^{3+}$-ions as well as cooling down to 77 K were necessary to obtain upconversion lasing in the visible spectral range [4].

The most suitable host crystals for the $Er^{3+}$-ion are fluorides, because they exhibit a low phonon energy which prevents the intraionic non-radiative decay of the relevant emitting and intermediate energy levels [5,6]. For this reason, upconversion lasers based on the fluoride hosts $LiYF_4$ and $KYF_4$ were more efficient than those utilizing $Y_3Al_5O_{12}$ as host material [7].

In erbium-doped materials the upconversion process is either an intraionic or an interionic process. The intraionic process takes place when two photons of the same wavelength are successively absorbed by the same ion in two steps. In this case, first GSA takes place, followed by ESA. The interionic process implies that, after two ions have been excited by GSA, a non-radiative energy transfer converts the de-excitation energy of one ion into a higher excitation state of the other ion.

Three possible intraionic two-step excitation channels for $Er^{3+}$:$LiLuF_4$ are depicted in Fig. 1. For a low concentration of $Er^{3+}$-ions, intraionic processes are more likely than interionic processes [7]. In scheme A, the first photon at 970 nm populates the metastable $^4I_{11/2}$-multiplet (GSA), from which the absorption of a second photon into the $^4F_{7/2}$-multiplet (ESA) may take place. This multiplet decays then fast non-radiatively into the $^4S_{3/2}$-multiplet. The laser

*Abbreviations:* GSA, ground state absorption; ESA, excited state absorption; OPSL, optically-pumped semiconductor laser; SE, stimulated emission; ESR, excited state reabsorption.

* Corresponding author. Tel.: +49 (0)40 8998 5160.
*E-mail address:* fmoglia@physnet.uni-hamburg.de (F. Moglia).

http://dx.doi.org/10.1016/j.optmat.2015.01.004
0925-3467/

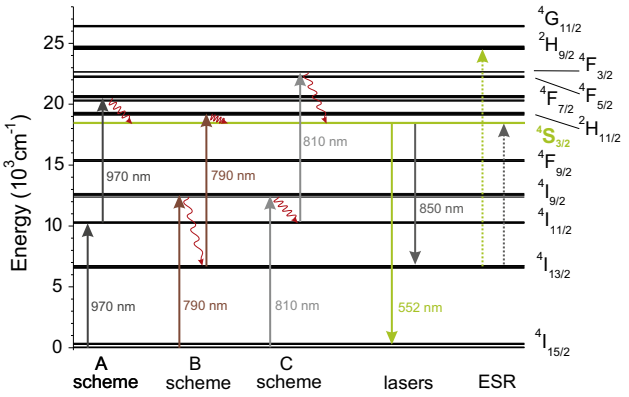


**Fig. 1.** $Er^{3+}$:$LiLuF_4$ energy-level diagram [9] and the ESA-pumping processes for laser emission at 552 nm and at 850 nm. Red waved arrows represent fast non-radiative decays. Dashed arrows show possible ESR processes of laser photons. (For interpretation of the references to colour in this figure legend, the reader is referred to the web version of this article.)

transition at 552 nm occurs from the $^4S_{3/2}$-multiplet into the thermally coupled upper multiplet level of the $^4I_{15/2}$ ground state.

Pump schemes B and C require a pump source at 790 nm (B) and 810 nm (C) [8,6], respectively. However, these schemes only allow for a theoretical maximum photon-energy conversion of 72% and 73%, respectively, which is lower than the maximum energy conversion of 88% regarding scheme A. This trend was also confirmed by experimental results, which showed the highest efficiency for green upconversion lasers pumped according to scheme A [10,11].

A second laser transition at around 850 nm is also possible following the decay $^4S_{3/2} \rightarrow {}^4I_{13/2}$ (Fig. 1). For this laser, the pumping scheme B is more favorable, as it depletes the long-living laser terminal level (see Section 2).

The most common upconversion laser material is $Er^{3+}$:$LiYF_4$, but even more efficient cw upconversion bulk lasers have been obtained with $Er^{3+}$:$LiLuF_4$ [12]. $LiLuF_4$ is isomorphic to $LiYF_4$ ($Lu^{3+}$-ions substitute $Y^{3+}$-ions) and, when doped with $Er^{3+}$-ions, shows comparable spectroscopic features. $Er^{3+}$:$LiLuF_4$ crystals have been pumped with either a Ti:sapphire laser or an OPSL [12,13]. In these experiments, a high pump fluence was required for the ESA-pumping process in order to obtain a reasonable efficiency.

Detrimental interionic processes quench the lifetime of the laser emitting multiplet at high $Er^{3+}$-concentrations. Therefore, we used low-doped (<1.5 at.%) $Er^{3+}$:$LiLuF_4$ crystals in this work.

With respect to the requirement of a high pump fluence, waveguide geometries could be beneficial for upconversion lasers. The first demonstration of an erbium-based upconversion laser in ZBLAN fibers has been reported by Whitley et al. [14]. An alternative approach is the waveguide inscription by writing multiple tracks with femtosecond-laser pulses defining a cladding buried inside a crystalline material, as demonstrated in $Nd^{3+}$:YAG [15]. In this case, one benefits from the advantage of the waveguiding geometry as well as from the superior spectroscopic and thermo-mechanical properties of crystals compared to glasses.

In this paper, we present the spectroscopic analysis of GSA and ESA at possible pump wavelengths of $Er^{3+}$:$LiLuF_4$ in order to understand and further underline its suitability as an upconversion-laser medium. Additionally, the influence of ESA at the laser emission wavelengths is considered. It will be demonstrated that the occupation of the involved energy levels varies for different regimes (under spectroscopic and lasing conditions). Although the cw-ESA spectrum does not show net gain at the laser wavelength (see Section 2), cw lasing is possible when the material is placed in a resonant cavity (see Section 3). Afterwards, laser experiments with more than 750 mW of cw output power are presented. This represents to the best of our knowledge, the highest cw output power of any room-temperature crystalline upconversion laser. Moreover, the first crystalline upconversion waveguide laser is presented.

## 2. Spectroscopic analysis

In order to realize an upconversion laser pumped by a single wavelength, a resonance between GSA and ESA must be present. The region around 970 nm is the most efficient pumping channel regarding photon energy conversion (see scheme A in Fig. 1). Spectroscopic measurements have been carried out in the spectral regions of pump and potential laser emission wavelengths, where ESA either favors or could be detrimental for the emission performance of the lasers.

For all the spectroscopic investigations an *a*-cut sample of an $Er^{3+}$:$LiLuF_4$ crystal fabricated by *AC Materials* has been employed. It had an $Er^{3+}$-concentration of 1.3 at.% and a length of 10 mm.

The polarization-dependent GSA spectra have been recorded with a *Varian* Cary 5000 UV–vis–NIR spectrophotometer. GSA cross sections have been derived by employing the Lambert–Beer law.

The setup to measure polarization-dependent ESA spectra was based on the one developed by Koetke and Huber [16]. The probe beam consisted of a white light source emitting a broad spectrum between 440 nm and 1750 nm (assembled system of FemtoPower 1060 and SC450-PP-HE by *Fianium*). The pump beam was delivered by a tunable cw Ti:sapphire laser (*Spectra Physics*), emitting a maximum output power of ~3.5 W in the investigated wavelength range. Spectra were recorded for different pump wavelengths between 967 nm and 975 nm and combined to one spectrum. In this way saturation artifacts due to scattered pump light were eliminated. As specified in [16], the obtained spectra are a superposition of GSA, SE, and ESA characteristics in dependence of the occupation of the involved energy levels. Nevertheless, in spectral regions where only GSA is present, a calibration of the total excitation density can be performed by comparing the respective GSA peaks with the previously determined GSA cross sections. Afterwards, the GSA characteristics can be subtracted from the spectrum. What remains is a superposition of ESA and SE characteristics, where dominating ESA yields negative values and dominating SE yields positive values. For simplicity, in this work this superimposed ESA and SE spectrum is named ESA spectrum and the label $\sigma_{ESA}$ on the *y*-axes in Figs. 2 and 3 represents the effective cross section, namely:

$$\sigma_{ESA} = \sum_i \frac{n_i}{n_e}(\sigma_{SE,i} - \sigma_{ESA,i}) \quad \text{with} \quad \sum_i n_i = n_e, \tag{1}$$

where $n_i$ are the population densities of the excited states, $n_e$ is the total excitation density and $\sigma_{SE,i}$ and $\sigma_{ESA,i}$ are the SE and the ESA cross sections of the excited states, respectively. Fig. 2 displays the GSA and effective ESA spectra of $Er^{3+}$:$LiLuF_4$ for $\pi$- and $\sigma$-polarizations in the wavelength range around 970 nm. The spectral resolution was 0.6 nm, which is comparable to the minimum width of the spectral features. Both, the GSA and ESA cross sections are higher in $\pi$-polarization. To find the optimum pump wavelength, an effective ESA-pump cross section $\sigma_{pump}$ was defined as:

$$\sigma_{pump} = \sqrt{-\sigma_{ESA} \cdot \sigma_{GSA}}. \tag{2}$$

The maximum of the product between $\sigma_{GSA}$ and $\sigma_{ESA}$ gives an indication of the highest ESA-pumping efficiency. The square root averages the product to a quantity that has the unit of a cross section. The minus compensates for the chosen negative sign of $\sigma_{ESA}$ for dominating ESA cross sections in Fig. 2. The highest values of $\sigma_{pump}$ are: $6.0 \cdot 10^{-21}$ cm$^2$ at $\lambda_{P1} = 974.2$ nm and $5.3 \cdot 10^{-21}$ cm$^2$ at $\lambda_{P2} = 972.0$ nm in $\pi$-polarization as well as $2.6 \cdot 10^{-21}$ cm$^2$ at

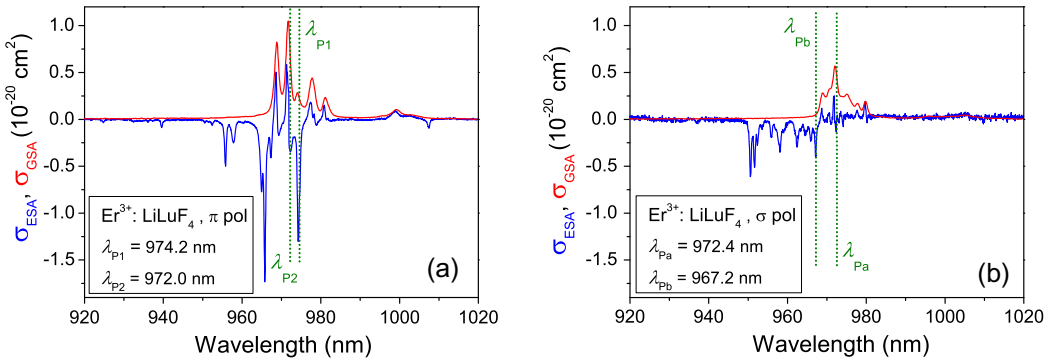


**Fig. 2.** ESA spectra in $Er^{3+}$:$LiLuF_4$ in $\pi$- (a) and $\sigma$-polarization (b). $\lambda_{P1}$, $\lambda_{P2}$ and $\lambda_{Pa}$, $\lambda_{Pb}$ are for both polarizations the two wavelengths presenting the highest effective ESA-pump cross sections $\sigma_{pump}$ (see text).

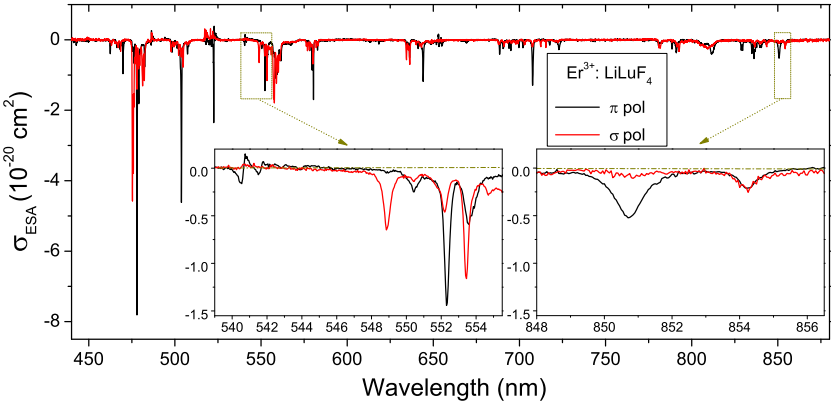


**Fig. 3.** ESA measurements in $Er^{3+}$:$LiLuF_4$ in $\pi$- and $\sigma$-polarization in the spectral range between 440 nm and 880 nm. In the first inset, the green spectral range around the possible laser wavelengths is highlighted. In the second inset, the spectral range around 850 nm, the other possible laser emission spectral range, is shown. (For interpretation of the references to colour in this figure legend, the reader is referred to the web version of this article.)

$\lambda_{Pa} = 972.4$ nm and $1.5 \cdot 10^{-21}$ $cm^2$ at $\lambda_{Pb} = 967.2$ nm in $\sigma$-polarization. The spectra depicted in Fig. 2(a) are similar to those reported for $\pi$-polarization in [12,13] and also to the spectral characteristics of $Er^{3+}$:$LiYF_4$ [16]. However, the higher resolution of the spectra reported here allows for a more precise refinement of the ESA cross sections as the narrow peaks are nearly fully resolved. Moreover, this is the first time that $\sigma$-polarized ESA spectra for $Er^{3+}$:$LiLuF_4$ are presented (Fig. 2(b)).

In contrast to desired ESA at the pump wavelength, ESA is detrimental when it occurs at the laser emission wavelength. In Fig. 3 the polarization-dependent ESA spectra in the spectral region between 440 nm and 880 nm for $Er^{3+}$:$LiLuF_4$ are shown. The resolution of 0.15 nm is higher than for the spectra previously reported in [17]. The first inset shows a slightly negative ESA signal at the expected laser emission wavelengths (540.6 nm, 551.6 nm and 552.6 nm, see Section 3) predicting at a first glance that cw laser emission should not be possible. However, we will show that such an interpretation is not correct.

In time-resolved ESA spectra of $Er^{3+}$:$LiYF_4$ for time intervals shorter than the radiative lifetime of the emitting $^4S_{3/2}$-multiplet ($\tau = 400$ µs), in fact SE is the dominant process around $\lambda = 552$ nm [17]. For longer time intervals ($t > \tau$), ESA becomes the dominant process. So, only pulsed upconversion lasing should be possible without ESA complications. The spectra in Figs. 2 and 3 are valid for $t \gg 2$ ms and thus compatible with the results reported for long time intervals in [17]. The variation in dependence of time of such ESA spectra demonstrates how the population densities of the involved energy levels can change even under spectroscopic conditions. According to these considerations, the measurements under spectroscopic conditions show that at least pulsed-laser operation in the green spectral range should be possible.

Nevertheless, in $Er^{3+}$:$LiYF_4$ even cw upconversion laser emission in the green spectral range can be obtained [7]. In [11,17], the reabsorption of photons at the laser wavelength from excited energy levels, ESR, has been recognized as probable transition in $Er^{3+}$:$LiYF_4$. The intermediate $^4I_{13/2}$-multiplet is populated by non-radiative decay from upper energy levels because of its relatively long lifetime of 10 ms. This may allow for efficient ESR at the laser wavelength via the transition $^4I_{13/2} \rightarrow {}^2H_{9/2}$ (see Fig. 1). Although the corresponding cross sections should be low due to the forbidden spin-flip required for this transition, ESR might become strong due to an increasing population density $n_{^4I_{13/2}}$ under cw excitation. The change of $n_i$ under spectroscopic conditions then leads to the negative $\sigma_{ESA}$ signal at the laser wavelengths observed in Fig. 3. The adopted pumping scheme A (see Fig. 1) efficiently depopulates the intermediate $^4I_{11/2}$-multiplet. Thus, its contribution to the detected ESR in the green spectral range should be much lower than that of the $^4I_{13/2}$-multiplet. Due to the small ESR probe-signal strength during spectroscopic investigations, the recycling effect to the upper laser multiplet $^4S_{3/2}$ (via $^2H_{9/2}$) is small in the ESA measurements, yielding a negligible effect on the population densities $n_i$. However, $n_i$ are expected to be significantly different under lasing conditions, when a strong photon flux at the laser wavelength is present.

Simulations performed for this work and previously [18] about $Er^{3+}$:$LiLuF_4$ and more recent works about $Er^{3+}$:$LiYF_4$ by Toma et al. [19,20] describe the conditions for pure cw operation of the laser in the green spectral range and the possible conflict with emission

around $\lambda = 850$ nm, as well including the earlier mentioned ESR transition $^4I_{13/2} \rightarrow {}^2H_{9/2}$ at 552 nm. The solutions of the rate equations of the system reveal the contribution of the laser photon flux. During laser experiments, the existing photon flux at the laser transition $^4S_{3/2} \rightarrow {}^4I_{15/2}$ can saturate the ESR-loss and enhance the recycling efficiency into the $^4S_{3/2}$-multiplet, allowing for cw laser operation. Consequently, although Toma et al. did not compare their conclusions with the apparently contradicting spectroscopic results, this explains why – despite the presence of ESR – cw laser operation is still possible. By an appropriate evaluation of the population densities $n_i$ under lasing conditions, one could in principle rescale the proportion between ESA and SE spectra in Fig. 3. It is evident that a total negative signal of only roughly $1 \cdot 10^{-21}$ cm$^2$ showing the dominance of ESR against SE in the green spectral range under spectroscopic conditions can easily become positive under lasing conditions. Even a slight bleaching of the ESR from the $^4I_{13/2}$-multiplet can lead to an increase of the occupation of the laser-emitting $^4S_{3/2}$-multiplet via recycling and consequently to a slight enhancement of SE. Absolute ESA and SE cross sections have been reported in [21]. However, the authors did not consider the population densities of the involved energy levels and their variation. Consequently, it is not possible to draw a direct comparison with the measurements reported here.

In $Er^{3+}$-doped fluoride crystals, laser emission is also possible around 850 nm on the transition $^4S_{3/2} \rightarrow {}^4I_{13/2}$. In this case, the preferable way to populate the laser-emitting $^4S_{3/2}$-multiplet is via the pumping process B in Fig. 1. The pump-ESA process starting from the long-living final $^4I_{13/2}$-multiplet promotes its depletion and favors a laser process which would be otherwise self-terminating [8,22]. Nevertheless, theoretical works about $Er^{3+}$:$LiYF_4$ demonstrate that also at 850 nm cw laser emission is possible with a high threshold when the pumping scheme A in Fig. 1 is adopted [23]. Additionally, laser competition between green and the 850 nm laser emission can occur [20]. The second inset in Fig. 3 shows that also around 850 nm ESR is present. As for the green laser emission, this process starts with the highest probability from the $^4I_{13/2}$-multiplet. The spectra in Fig. 3 show the situation under spectroscopic conditions, which means at a specific occupation of the involved energy levels. If a laser photon flux at around 850 nm is considered for the transition $^4S_{3/2} \rightarrow {}^4I_{13/2}$, the reversed transition $^4I_{13/2} \rightarrow {}^4S_{3/2}$ is similar to the GSA reabsorption process that a quasi-three-level laser experiences. Consequently, the laser can run at this wavelength, but the laser threshold is higher than in absence of the ESR process. One can expect that during spectroscopic measurements for short excitation times, SE is dominant also in the 850 nm spectral range.

In conclusion, the spectroscopic investigations have revealed that a pump wavelength of 974.2 nm in $\pi$-polarization is needed for the most effective resonance between ESA and GSA in $Er^{3+}$:$LiLuF_4$. It has been shown that under spectroscopic conditions with relatively long time scales ESR processes are present on both possible laser-emission-wavelength regions of $Er^{3+}$:$LiLuF_4$ upconversion lasers. Nevertheless, under lasing conditions with a laser photon flux being present, the population densities of the involved energy levels are different. ESR processes can be bleached and the population can be recycled into the laser-emitting level. Consequently, such as in $Er^{3+}$:$LiYF_4$, efficient cw lasing is possible also in $Er^{3+}$:$LiLuF_4$.

## 3. Laser experiments

### 3.1. Experiments with bulk crystals

As mentioned above, a high pump fluence is essential for upconversion lasers based on $Er^{3+}$:$LiLuF_4$ crystals. Due to its good beam quality, a Ti:sapphire laser allows for tight focusing and thus for a high pump intensity. Another approach to achieve high pump power at a good beam quality in the required wavelength range is the use of OPSLs based on GaAs–InGaAs [24].

The previously described Ti:sapphire laser as well as a more powerful OPSL (*Coherent*) with a maximum output power of about 10 W and a tunability range of roughly 20 nm between 960 nm and 980 nm were thus employed as pump sources.

First, upconversion laser emission was obtained in a hemispherical resonator geometry when pumping with the Ti:sapphire laser. After a focusing lens with $f = 40$ mm, a flat input coupling mirror was positioned almost in contact with a 1.0 at.%-$Er^{3+}$-doped, 2.40 mm-long $LiLuF_4$ crystal. The mirror was coated highly transmissive for the pump wavelength and highly reflective for the laser wavelength at 551.6 nm. Output coupling mirrors with a radius of curvature of 50 mm and different transmissions between 1.0% and 5.8% at the laser wavelength were employed. A reflectivity exceeding 85% for all output coupling mirrors at the pump wavelength ensured a double-pass pumping. The length of the sample allowed for a good overlap between both pump and laser beams with a beam waist of roughly 30 μm, ensuring the required high pump intensity. When pumping at $\lambda_{P1} = 974.2$ nm (see Section 2), an absorption of 13% per single-pass was measured at the laser threshold and an absorption efficiency of 24% per double pass was estimated, considering the further bleaching of the crystal during the second pass. In Fig. 4(a) the output power is plotted versus absorbed pump power. A maximum slope efficiency of 20.7% and an output power of almost 80 mW at a laser wavelength of $\lambda_{L1} = 551.6$ nm was achieved with an output coupling transmission of 4.1%. The absorption efficiency and the maximum output power are comparable with results presented previously in a similar setup [12], while the laser threshold has been lowered to less

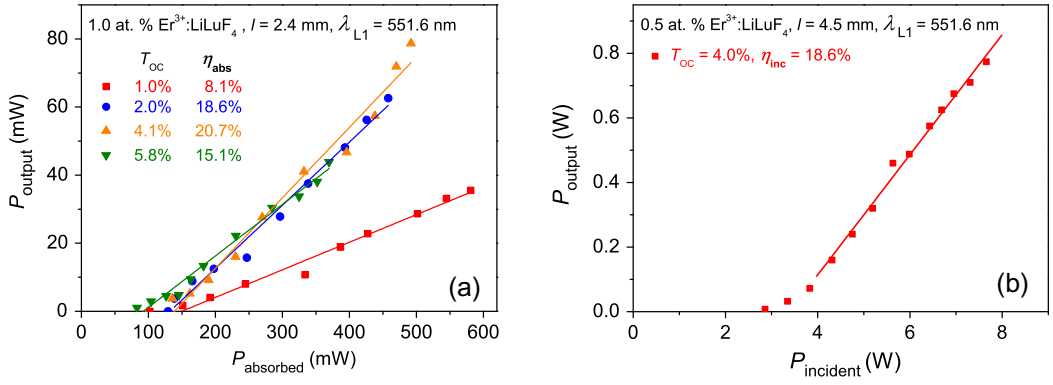


**Fig. 4.** Upconversion-laser input–output curves with $Er^{3+}$:$LiLuF_4$ crystals. In (a), the laser emission at $\lambda_{L1} = 551.6$ nm with respect to the absorbed pump power in a twofold hemispherical resonator with the Ti:sapphire laser as pump source is reported. In (b), the laser emission with respect to the incident pump power in a fourfold laser cavity with the OPSL as pump source is shown.

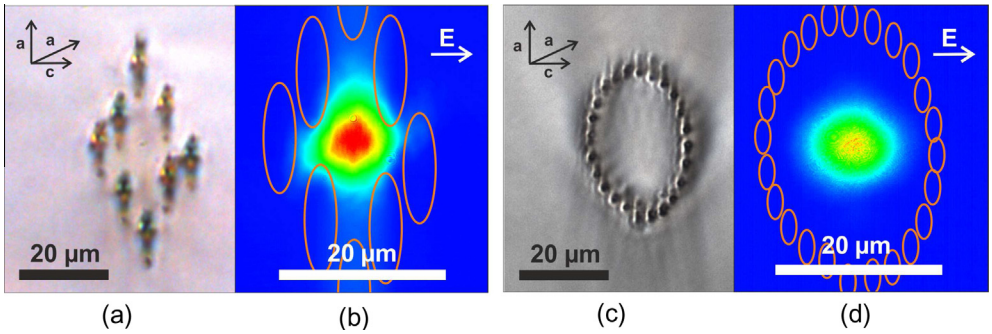


**Fig. 5.** Rhombic and elliptical claddings inscribed into 1.3 at.% $Er^{3+}$-doped $LiLuF_4$ crystals. In (a) and (c), microscope pictures of the rhombic and elliptical structures are depicted. In (b) and (d), an image of the guided mode of a HeNe laser is shown for a rhombic and an elliptical cladding, respectively. The direction of the electric field vector **E** parallel to the **c**-axis is also shown.

than 130 mW of absorbed pump power or 680 mW of incident pump power.

To increase the absorption efficiency, a longer crystal was employed in the hemispherical resonator already presented in [12]. In this setup, four passes are realized by a suitable coating on the two facets of the crystal and a hole in the input coupling mirror of the concentric cavity.

Substituting the Ti:sapphire laser by an OPSL as pump source, the performance could be considerably increased in terms of maximum pump and output power. Previously, at absorbed pump powers higher than 1 W thermal problems arose and a pump duty cycle of 50% had to be imposed [13].

In order to solve these thermal issues, in the fourfold resonator, a 0.5 at.% $Er^{3+}$-doped $LiLuF_4$ crystal with a length of 4.5 mm was mounted on a copper heat sink which was cooled by a Peltier element set to a temperature around 20 °C. The crystal presents a good combination of low $Er^{3+}$-doping concentration (roughly a half than in former experiments) and roughly three times extended length. In this way, we obtained a high absorption efficiency as well as still a good overlap of pump and laser beams. The experiments carried out with this new setup are presented in Fig. 4(b). Applying an output coupling transmission of 4.1%, a maximum output power of 774 mW in pure cw operation was obtained at $\lambda_{L1} = 551.6$ nm with a slope efficiency of 18.6% with respect to the incident pump power of the OPSL at a pump wavelength of $\lambda_{P1} = 974.2$ nm. The laser threshold was reached at 2.9 W of incident pump power and the overall optical-to-optical efficiency was overcoming 10%. The slope efficiency with respect to the absorbed pump power was estimated to be as high as 59%.

### 3.2. Waveguide fabrication and waveguide lasers

As previously mentioned, the waveguide geometry is advantageous to provide the required pump intensity for efficient upconversion laser operation, as the light confinement ensures a very good overlap between pump and laser modes. Moreover, it offers a convenient way of miniaturization of the system.

Femtosecond-laser-written waveguides have been proven to be suitable for highly efficient laser operation also in the visible spectral range [25]. Furthermore, visible laser operation was demonstrated in femtosecond-laser-written waveguides inscribed in a $Pr^{3+}$-doped $LiYF_4$ crystal [26]. Therefore, the same rhombic cladding geometry has been inscribed into a 1.3 at.% $Er^{3+}$-doped, -long $LiLuF_4$ crystal. A chirped-pulse-amplification femtosecond-laser system (*Clark-MXR CPA-2010*) with a center wavelength of 775 nm, a repetition rate of 1 kHz, a pulse duration of 160 fs, and a pulse energy up to 1 mJ has been employed. Eight parallel tracks have been inscribed, choosing a pulse energy of 0.6 μJ and a writing velocity of 25 μm/s.

For a second sample, a -long, 1.3 at.% $Er^{3+}$-doped $LiLuF_4$ crystal, the writing procedure has been optimized increasing the number of the inscribed tracks to twenty-four in an elliptical shape, but reducing the pulse energy to 0.3 μJ and increasing the writing velocity to 250 μm/s. In both crystals, the claddings have been inscribed along one of the **a**-axes in order to address the $\pi$-polarization with its higher cross sections for the laser experiments. In our first attempts both kinds of claddings had dimensions of approximately $20 \times 30$ μm$^2$. The corresponding microscope pictures are shown in Fig. 5(a) and (c).

To investigate the waveguiding properties of such structures, the beam of a polarized HeNe-laser at 632.8 nm was coupled into the waveguides and transmission measurements have been performed. Additionally, the near-field guided mode was imaged via a 50× microscope lens onto the chip of a CCD camera (*DAT-WinCamD-UCD15*).

In both claddings, the waveguiding was polarization-dependent: only light in $\pi$-polarization was guided. The mode profiles are shown in Fig. 5(b) and (d) for the rhombic and elliptical structures, respectively.

The advantage in using the elliptical instead of the rhombic claddings is the much lower waveguide loss. In the case of the rhombic waveguides, a damping below 5.3 dB/cm has been evaluated, while in the elliptical claddings it was below 0.5 dB/cm, which is a promising value, when compared to similar structures [27]. Both dampings represent maximum values with the assumption of an ideal incoupling efficiency of 100% of the HeNe-laser beam into the waveguides.

In the resonator depicted in Fig. 6(a), the radiation of the Ti:sapphire laser at $\lambda_{P1} = 974.2$ nm was coupled into the waveguides via a microscope objective lens ($10\times, NA = 0.22$), which also represented an intracavity lens for realizing a stable resonator. The two flat mirrors $M_1$ and $M_2$ constituted the cavity. $M_1$ was ideally antireflective and $M_2$ highly reflective at the pump wavelength, while their transmission at the laser wavelength determined the total outputcoupling transmission. The total power emission corresponded to the sum of $P_2$, deflected by $M_3$ (highly transmissive at the pump wavelength and highly reflective at the laser wavelength), and $P_1$, which was imaged onto a powermeter sensor by a second microscope objective lens ($50\times, NA = 0.5$).

With the rhombic cladding, the first crystalline green upconversion waveguide laser has been realized. However, the laser emission at $\lambda_{L2} = 540.6$ nm was unstable and spiky with a quasi-cw behavior. True-cw laser operation at $\lambda_{L1} = 551.6$ nm has been recorded.

These results could be improved by adopting the elliptical waveguides. Green cw laser emission has been obtained at $\lambda_{L3} = 552.6$ nm with a maximum output power of 10 mW. The

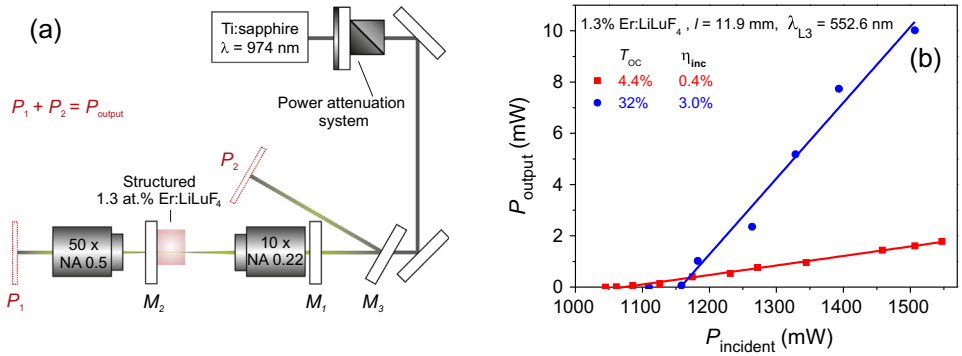


**Fig. 6.** Upconversion lasers in waveguides inscribed in 1.3 at.% $Er^{3+}$-doped $LiLuF_4$ crystals. In (a), the setup for the laser experiments is reported. The total output power is the sum between the two contributions $P_1$ and $P_2$. In (b), the laser emission in the green spectral range with respect to the incident pump power for two different total output coupling transmissions in elliptical waveguides is shown. (For interpretation of the references to colour in this figure legend, the reader is referred to the web version of this article.)

input–output curves depicted in Fig. 6(b) refer to a total output coupling transmission of 4.4% and 32%, respectively.

As predicted in [20], laser emission at $\lambda_{L4} = 849.8$ nm could be also achieved in both waveguides. In this case the laser output was detectable, but unstable when operated without mirrors. Thus, two plane mirrors $M_1$ and $M_2$ with nominal transmissions of 93.2% and 93.4% at the laser wavelength, respectively were employed as an external resonator. In this configuration, a maximum average output power of 10 mW could be achieved in an elliptical cladding. Nevertheless, the laser output was self-pulsed in all laser experiments at this wavelength.

## 4. Conclusions

We performed detailed spectroscopic investigations of the upconversion laser material $Er^{3+}$:$LiLuF_4$ with particular focus on excited state absorption. The results prove that a pump wavelength of 974.2 nm allows for an efficient population of the upper laser multiplet $^4S_{3/2}$ via ESA. In these investigations ESR appears to be the dominating process at the laser wavelengths around 552 nm and 850 nm. This outcome seems to be in contradiction to the laser results here and in previous reports [6–8]. However, Toma et al. [19,20,23] found steady state solutions for a rate equation system implementing all involved energy levels and probable ESR transitions at the laser wavelengths in $Er^{3+}$:$LiYF_4$. From these results, we conclude that the ESR from the long-living intermediate $^4I_{13/2}$-multiplet is bleached at high photon densities present in laser resonators. As a consequence, at least for $Er^{3+}$:$LiYF_4$ and $Er^{3+}$:$LiLuF_4$, but possibly also for other $Er^{3+}$-doped materials, efficient cw lasing is possible despite a negative outcome of the ESA spectroscopy. Future spectroscopic investigations focusing on ESA will have to take this into account by evaluating the occupation of the involved energy levels in the lasing regime and possibly record ESA spectra at high probe intensity.

In upconversion-laser experiments employing a 1.0 at.%-doped $Er^{3+}$:$LiLuF_4$ crystal in a hemispherical-resonator configuration, promising results with laser output powers of up to 80 mW at a laser wavelength of 551.6 nm were obtained. A slope efficiency exceeding 20% was achieved under Ti:sapphire pumping at 974.2 nm. Further experiments in a multi-pass cavity allowed for an improved output power of up to 774 mW under pumping with an OPSL. To the best of our knowledge, this represents the highest cw output power of any room-temperature crystalline upconversion laser. The slope efficiency with respect to the absorbed pump power exceeding 50% even in a conservative estimation reveals the great potential for a further increase of the output power.

Finally, crystalline femtosecond-laser-written waveguides with rhombic and elliptical cladding configurations have been inscribed into 1.3 at.%-doped $Er^{3+}$:$LiLuF_4$ crystals. For the waveguides with an elliptical cladding, the transmission of the fundamental mode of a HeNe laser was measured to be below 0.5 dB/cm. This value is low compared to similar structures previously reported [27]. In this configuration, cw-laser output at 552.6 nm and self-pulsed output at 849.8 nm with a maximum output power of 10 mW in both cases were obtained under Ti:sapphire pumping. We demonstrated the first crystalline upconversion waveguide lasers to the best of our knowledge and the first step towards miniaturization of the system. Further steps would be the use of diode-laser pump sources, direct mirror coatings on the waveguide endfacets and more compact incoupling-lens systems.

## Acknowledgements

The authors thank M. Eichhorn and M. Schellhorn for providing the crystal for spectroscopic investigations and acknowledge financial support of the Joachim Herz Stiftung in the frame of the Landesexzellenzinitiative “Frontiers in Quantum Photon Science”.

## References

[1] R.M. Macfarlane, F. Tong, A.J. Silversmith, W. Lenth, Violet cw neodymium upconversion laser, Appl. Phys. Lett. 52 (1988) 1300–1302.
[2] D.C. Nguyen, G.E. Faulkner, M. Dulick, Blue–green (450 nm) upconversion $Tm^{3+}$:YLF laser, Appl. Opt. 28 (1989) 3553–3555.
[3] M.E. Koch, A.W. Kueny, W.E. Case, Photon avalanche upconversion laser at 644 nm, Appl. Phys. Lett. 56 (1990) 1083–1085.
[4] L.F. Johnson, H.J. Guggenheim, Infrared-pumped visible laser, Appl. Phys. Lett. 19 (1971) 44–47.
[5] F.K. Fong, S.L. Naberhuis, M.M. Miller, Theory of radiationless relaxation of rare-earth ions in crystals, J. Chem. Phys. 56 (1972) 4020–4027.
[6] H. Scheife, G. Huber, E. Heumann, S. Bär, E. Osiac, Advances in up-conversion lasers based on $Er^{3+}$ and $Pr^{3+}$, Opt. Mater. 26 (2004) 365–374.
[7] R. Brede, E. Heumann, J. Koetke, T. Danger, G. Huber, B. Chai, Green up-conversion laser emission in Er-doped crystals at room temperature, Appl. Phys. Lett. 63 (1993) 2030–2031.
[8] P.E.-A. Möbert, E. Heumann, G. Huber, 540 mW of blue output power at 425 nm generated by intracavity frequency doubling an upconversion-pumped $Er^{3+}$:$LiYF_4$ laser, Appl. Phys. Lett. 73 (1998) 139–141.
[9] A.A. Kaminskii, Stimulated emission spectroscopy of $Ln^{3+}$ ions in tetragonal $LiLuF_4$ fluoride, Phys. Status Solidi A 97 (1986) K53–K60.
[10] T. Hebert, R. Wannemacher, W. Lenth, R.M. Macfarlane, Blue and green cw upconversion lasing in Er:$LiYF_4$, Appl. Phys. Lett. 57 (1990) 1727–1729.
[11] M. Pollnau, W. Lüthy, H.P. Weber, Population mechanisms of the green $Er^{3+}$:$LiYF_4$ laser, J. Appl. Phys. 77 (1995) 6128–6134.
[12] E. Heumann, S. Bär, H. Kretschmann, G. Huber, Diode-pumped continuous-wave green upconversion lasing of $Er^{3+}$:$LiLuF_4$ using multipass pumping, Opt. Lett. 27 (2002) 1699–1701.

[13] E. Heumann, S. Bär, K. Rademaker, G. Huber, S. Butterworth, A. Diening, W. Seelert, Semiconductor-laser-pumped high-power upconversion laser, Appl. Phys. Lett. 88 (2006) 061108–061108-3.
[14] T.J. Whitley, C.A. Millar, R. Wyatt, M.C. Brierley, D. Szebesta, Upconversion pumped green lasing in erbium doped fluorozirconate fibre, Electron. Lett. 27 (1991) 1785–1786.
[15] A.G. Okhrimchuk, A.V. Shestakov, I. Khrushchev, J. Mitchell, Depressed cladding, buried waveguide laser formed in a YAG:$Nd^{3+}$ crystal by femtosecond laser writing, Opt. Lett. 30 (2005) 2248–2250.
[16] J. Koetke, G. Huber, Infrared excited-state absorption and stimulated-emission cross sections of $Er^{3+}$-doped crystals, Appl. Phys. B 61 (1995) 151–158.
[17] T. Danger, J. Koetke, R. Brede, E. Heumann, G. Huber, B.H.T. Chai, Spectroscopy and green upconversion laser emission of $Er^{3+}$-doped crystals at room temperature, J. Appl. Phys. 76 (1994) 1413–1422.
[18] G. Huber, Visible cw solid-state lasers, in: D.M. Finlayson, B.D. Sinclair (Eds.), Advances in Lasers and Applications, Scottish Universities School in Physics and Institute of Physics Publishing, Bristol, 1999, pp. 19–38.
[19] O. Toma, Emission regimes of a green $Er^{3+}$:$LiYF_4$ laser, IEEE J. Quantum Elect. 43 (2007) 519–526.
[20] O. Toma, S. Georgescu, Competition between green and infrared emission in $Er^{3+}$:$LiYF_4$ upconversion lasers, Opt. Commun. 284 (2011) 388–397.
[21] C. Labbé, J.-L. Doualan, S. Girard, R. Moncorgé, M. Thuau, Absolute excited state absorption cross section measurements in $Er^{3+}$:$LiYF_4$ for laser applications around 2.8 μm and 551 nm, J. Phys-Condens. Mat. 12 (2000) 6943–6957.
[22] C.A. Millar, M.C. Brierley, M.H. Hunt, S.F. Carter, Efficient up-conversion pumping at 800 nm of an erbium-doped fluoride fibre laser operating at 850 nm, Electron. Lett. 26 (1990) 1871–1873.
[23] O. Toma, S. Georgescu, 850 nm emission in $Er^{3+}$:$LiYF_4$ upconversion lasers, Rom. J. Phys. 55 (2010) 790–799.
[24] M. Kuznetsov, F. Hakimi, R. Sprague, A. Mooradian, High-power (> 0.5-W CW) diode-pumped vertical-external-cavity surface-emitting semiconductor lasers with circular $TEM_{00}$ beams, IEEE Photonic. Tech. L. 9 (1997) 1063–1065.
[25] F. Reichert, T. Calmano, S. Müller, D.-T. Marzahl, M. Fechner, G. Huber, Efficient visible laser operation of Pr, Mg:$SrAl_{12}O_{19}$ channel waveguides, Opt. Lett. 38 (2013) 2698–2701.
[26] S. Müller, T. Calmano, P. Metz, N.-O. Hansen, C. Kränkel, G. Huber, Femtosecond-laser-written diode-pumped Pr:$LiYF_4$ waveguide laser, Opt. Lett. 37 (2012) 5223–5225.
[27] T. Calmano, S. Müller, Crystalline waveguide lasers in the visible and near-infrared spectral range, IEEE J. Sel. Top. Quant. 21 (2015) 1602213.